Volume 55 | Number 82 | 21 October 2019 | Pages 12269–12414

ChemComm

Chemical Communications

rsc.li/chemcomm

ISSN 1359-7345

ROYAL SOCIETY OF CHEMISTRY | Celebrating IYPT 2019

COMMUNICATION

Dmytro A. Yushchenko *et al.*

Nitrobenzyl-based fluorescent photocages for spatial and temporal control of signalling lipids in cells

ChemComm

COMMUNICATION

View Article Online
View Journal | View Issue

Cite this: *Chem. Commun.*, 2019, **55**, 12288

Received 19th July 2019,
Accepted 27th August 2019

DOI: 10.1039/c9cc05602e

rsc.li/chemcomm

Nitrobenzyl-based fluorescent photocages for spatial and temporal control of signalling lipids in cells†

Pankaj Gaur,‡[a] Oleksandr A. Kucherak,‡[a] Yulia G. Ermakova,[b] Volodymyr V. Shvadchak[a] and Dmytro A. Yushchenko *[ac]

Here we present a set of fluorescent cages prepared by tethering fluorescent dyes to a photolabile group. The developed molecules enable caging of signalling lipids, their delivery to specific cellular membranes, with further imaging, quantification, and controlled photorelease of active lipids in living cells.

Many cellular signalling pathways strongly rely on lipids. However, lipids exhibit dynamic intracellular behaviour. Lipids are metabolically interconvertible by lipid handling protein machinery,[1,2] and can quickly change their location.[3] Additionally, small variations in levels of signalling lipid lead to diverse downstream effects due to their tightly regulated and non-uniform subcellular distribution.[4,5] In this respect, chemical biology tools that permit modulation of lipid signalling events with high spatial and temporal precision are extremely important for investigation and understanding of the mechanisms of lipid signalling.[6]

The intracellular levels of signalling lipids may be rapidly manipulated by chemical[7,8] or optogenetic[9,10] protein modulation systems using small molecule or a flash of light, respectively. While proven to be valuable techniques, these protein modulation systems depend on the expression of recombinant proteins. Although, use of photoswitchable lipids may be the direct approach to manipulate lipid signalling events,[11–14] selective delivery of signalling lipids at a defined subcellular site still remains challenging. In this direction, photocaging can be an effective approach which is known to release bioactive molecules from their inactive precursors.[15–34] Recently, coumarin and *ortho*-nitrobenzyl (ONB) cages have been employed in studies of lipid signalling.[35–38] Coumarin cages are fluorescent and therefore allow the quantification of released lipids, meanwhile they suffer from unintended photorelease of lipids during imaging (leakage) due to same wavelength for imaging and uncaging. On the contrary, ONB cages are incapable of providing quantification of photoreleased lipids due to their non-fluorescent nature. Additionally, some cages bearing target-specific chemical moieties allowed the delivery of signalling lipids at defined subcellular sites.[39–42] Hence, the development of new photocages for lipid signalling investigations is necessary to overcome the limitations of existing tools.

In this work, by splitting the functions of uncaging and imaging into different units, we designed small molecules that allow spatial and temporal control on lipids' delivery, and precise quantification of photoreleased lipid. To achieve this, we covalently tethered photolabile ONB cage ($\lambda_{photocleavage}$ = 365 nm) and rhodamine dyes (Rh-dyes, λ_{ex} = 559 nm) to construct fluorescent photocages (ONB-Rh scaffolds). As reported, caged lipids bearing negatively charged sulfonate groups are selectively localized at the plasma membrane (PM) while neutral lipids mostly localized at internal membranes (IMs).[39] Therefore, we chose negatively charged Atto-532 and neutral sulfoRhB to selectively localize caged lipids at the PM and IMs, respectively (Fig. 1).

In addition, owing to the red-shifted emission, Rh-dyes could offer the possibility of live-cell imaging along with CFP- and GFP-based sensors for signalling molecules. As a signalling lipid, we chose oleic acid (OA) which serves as an agonist of free fatty acid receptor GPR40.[39,43,44] We synthesized two ONB cages bearing different linkers for dye conjugation starting from vanillin, and subsequently coupled those to OA by DCC mediated esterification. ONB caged-oleates were then tethered to Atto-532 and sulfoRhB to develop three caged-oleates PMC-OA, IMC-OA and IMC2-OA (Fig. 1 and Schemes S1, S2, ESI†).

We characterized the caged-oleates spectroscopically and as expected, their absorbance and emission properties were similar to those of the parent dyes Atto-532 and SulfoRhB (Fig. S1 and

[a] *Laboratory of Chemical Biology, The Institute of Organic Chemistry and Biochemistry of the Czech Academy of Sciences, Flemingovo namesti 2, 16610 Prague 6, Czech Republic. E-mail: yushchenko@uochb.cas.cz*
[b] *Cell Biology & Biophysics Unit, European Molecular Biology Laboratory (EMBL), Meyerhofstrasse 1, 69117 Heidelberg, Germany*
[c] *Group of Bioconjugation Chemistry, Miltenyi Biotec GmbH, Friedrich-Ebert-Straße 68, 51429 Bergisch Gladbach, Germany. E-mail: dmytroy@miltenyibiotec.de*

† Electronic supplementary information (ESI) available: Details of synthesis and characterization of caged lipids; control cell experiments. See DOI: 10.1039/c9cc05602e

‡ These authors contributed equally.

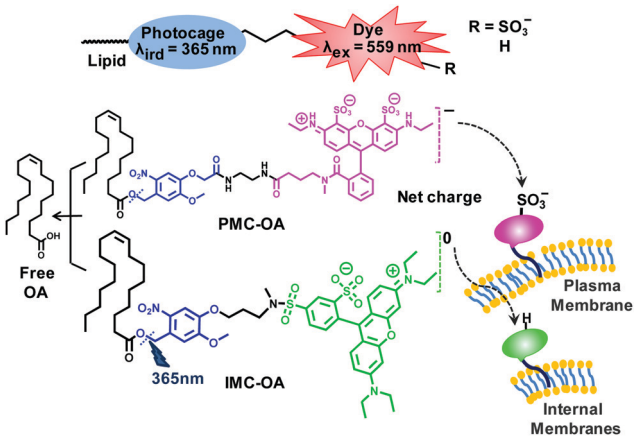

Fig. 1 Molecular design of fluorescent ONB-Rh caged-oleates.

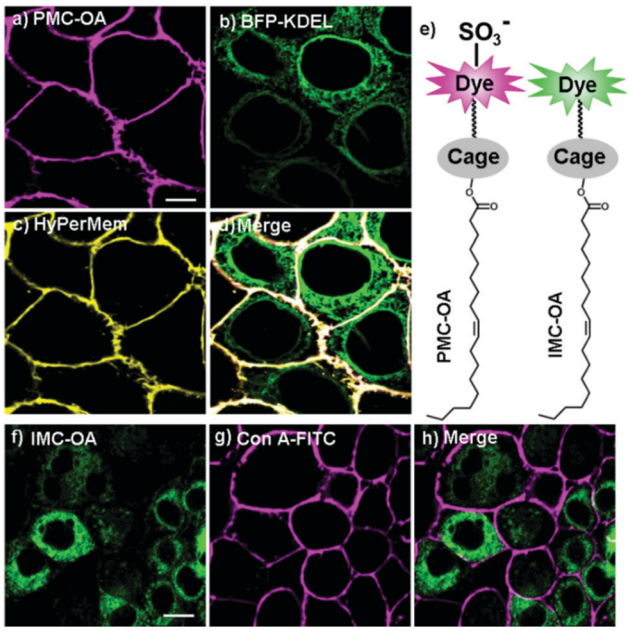

Fig. 2 Cellular localization of caged-oleates in live HeLa cells: (a) PMC-OA, λ_{ex} = 559 nm; (b) endoplasmic reticulum marker, λ_{ex} = 405 nm; (c) plasma membrane marker, λ_{ex} = 488 nm and (d) overlay of (a), (b) and (c) images; (e) caged-oleates; (f) IMC-OA, λ_{ex} = 559 nm; (g) plasma membrane tracker, λ_{ex} = 488 nm and (h) overlay of (f) and (g) images. Scale bar is 20 μm.

Table S1, ESI†). Next, to check whether uncaging of caged-oleates efficiently releases OA, we studied uncaging dynamics of IMC-OA in solution under exposure to 365 nm LED. The progress of uncaging reaction was monitored using thin layer chromatography (TLC). After 5 min of exposure TLC showed the complete uncaging of IMC-OA and the appearance of a spot with the same retention factor as free OA (Fig. S2, ESI†). Appearance of peak at m/z = 281.2 in the mass spectrum of exposed sample clearly revealed the photorelease of OA upon uncaging (Fig. S3, ESI†). Finally, the progress of uncaging was monitored by NMR analysis. The appearance of a new peak at 2.38 ppm corresponding to α-methylene of free OA and gradual decrease in the peak at 2.44 ppm upon exposure clearly validated the photorelease of OA upon uncaging (Fig. S4, ESI†).

We then checked the localization of caged-oleates in living cells by means of confocal fluorescence microscopy. Namely, we expressed endoplasmic reticulum marker BFP-KDEL[45] and PM marker HyPerMem[46] in HeLa cells and treated them with 30 μM PMC-OA. The fluorescence pattern of negatively charged PMC-OA completely overlapped with HyPerMem (Pearson's correlation coefficient = 0.94) which clearly demonstrated its selective localization at the PM (Fig. 2a–d). In contrast, neutral IMC-OA (45 μM) stained the IMs (Fig. 2f–h). However, IMC-OA showed excessive precipitation in imaging buffer. Then to check the impact of linker between ONB cage and rhodamine dye toward the water solubility, we synthesized IMC2-OA bearing the same linker as used in the case of PMC-OA. IMC2-OA (30 μM) was also localized at the IMs but exhibited better water solubility than IMC-OA (Fig. S5, ESI†), which clearly reflected the importance of polar linker to prevent lipid precipitation during delivery to cells.

Next, we checked the uncaging efficiency of OA in cells. HeLa cells loaded with PMC-OA were imaged on a dual scanner confocal microscope with controlled UV illumination during live-cell imaging. As expected, illumination with 375 nm light led to a significant decrease in the fluorescence intensity of PMC-OA in cells (Fig. 3a and b). The observed decrease may be caused by OA uncaging and the diffusion of released ONB-dye cage from the focal plane as described for coumarin-caged OA in the work of Nadler *et al.*[39] However, it does not directly prove the photorelease of free fatty acid. With the aim to confirm OA photorelease, we expressed free fatty acid receptor GPR40 in HeLa cells. This GPCR receptor in the presence of fatty acids is known to induce the elevation in intracellular Ca^{2+} levels[14] *via* activation of phospholipase C (PLC) as shown in Fig. 3e.[47] For monitoring intracellular Ca^{2+} levels we used genetically encoded green fluorescent GCaMP6s sensor,[48] which was co-expressed with GPR40. Thereafter, PMC-OA loaded cells were illuminated with 375 nm laser. A gradual increase in GCaMP6s fluorescence with the decrease in fluorescence intensity of PMC-OA (Fig. 3c and d) confirmed the photorelease of free OA.

We also performed a set of control experiments to validate the role of GPR40 activation in elevation of Ca^{2+} levels, and to rule out the possibility of any photogenerated artefact. Namely, we added free OA to HeLa cells expressing GCaMP6s and GPR40 that led to increase in intracellular Ca^{2+} levels (Fig. S6, ESI†). In contrast, no increase in Ca^{2+} levels was observed in cells expressing GCaMP6s only (no GPR40) upon addition of free OA (Fig. S6, ESI†) or upon uncaging of PMC-OA (Fig. S7, ESI†). Both experiments confirm that the main cause of the observed increase in intracellular Ca^{2+} levels is activation of GPR40 by free OA.

Next, cells expressing GCaMP6s and GPR40 were treated with precursor ONB cage and sulfoRhB separately. In both cases, irradiation with 375 nm laser did not lead to the increase in GCaMP6s fluorescence (Fig. S8, ESI†), which clearly revealed that the elevation in Ca^{2+} levels was the result of OA photorelease and not the result of any photogenerated artefacts.

To dissect uncaging from dye bleaching upon 375 nm irradiation, we used an earlier developed assay based on the comparison of decrease in fluorescence signal of cage at the PM

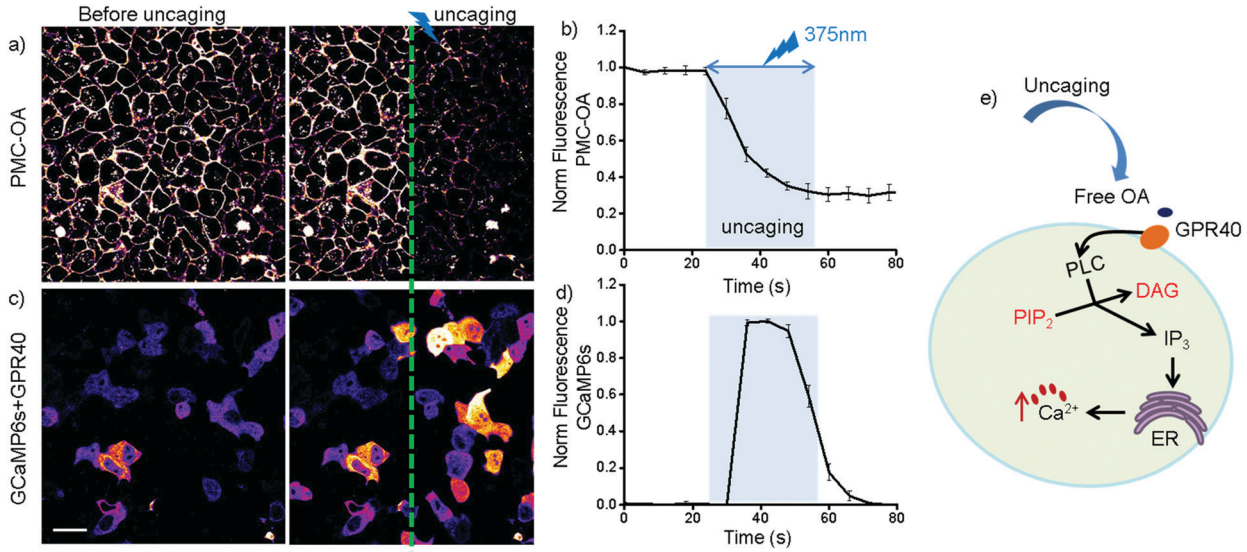

Fig. 3 (a and b) Change in fluorescence intensity of PMC-OA upon photouncaging using 375 nm laser. (c and d) Change in fluorescence intensity of calcium sensor GCaMP6s (λ_{ex} = 488 nm) in the response to photorelease of oleic acid. (e) Schematic representation of fatty acid induced elevation in intracellular Ca^{2+} levels. Error bars represent SD. Scale bar is 20 μm.

and endosomes.[39] Namely, HeLa cells were first incubated with PMC-OA for 10 min, then the loading solution was removed and cells were kept at 37 °C for 90–180 min to ensure partial endocytosis of caged lipid. Irradiation of these cells with 375 nm laser resulted in significant decrease of fluorescence signal of PMC-OA at the PM while much lower signal decrease in vesicles (Fig. S9, ESI†). These data correlate well with our previous results for coumarin-caged lipids[39] and the observed difference in fluorescence decrease between endosomes and the PM corresponds to the photorelease of OA.

Next, to compare the propensity of ONB-Rh and coumarin cages to the unintended uncaging during imaging, cells expressing GCaMP6s and GPR40 were loaded with PMC-OA and ScC-OA (OA caged with a coumarin group bearing two negatively charged sulfonate groups, compound **9** in ref. 39) separately. First, we imaged distribution of PMC-OA and ScC-OA using 559 nm and 405 nm excitation, respectively. Subsequently, we monitored variation in intracellular Ca^{2+} levels in both conditions using fluorescence of GCaMP6s (488 nm excitation). Elevation in Ca^{2+} levels under excitation of 405 nm laser in the case of ScC-OA was observed that clearly revealed the unintended release of lipid (leakage) during imaging (Fig. S10, ESI†). In contrast, unchanged Ca^{2+} levels in the case of PMC-OA demonstrated the stability of the ONB-dye scaffold to uncaging during imaging (Fig. S11, ESI†).

To further test the applicability of ONB-Rh cage in the presence of coumarin and vice-versa, we loaded the cells expressing GCaMP6s and GPR40 with both ScC-OA and PMC-OA. The cells were imaged upon illumination with 405 nm (0.5% laser power), and with 559 nm (1% power), to excite ScC-OA and PMC-OA respectively. The cells at left half of the imaged area were irradiated with 405 nm laser at 100% power. As expected, exposure to a strong 405 nm laser irradiation led to the uncaging of ScC-OA. However, PMC-OA exhibited no change in fluorescence intensity under illumination with 405 nm laser, meaning no photorelease (Fig. 4b and c). In contrast, irradiation of the cells at the right half of the imaged area with 375 nm laser resulted in the uncaging of both coumarin-caged and ONB-Rh-caged OA. Thus when used with coumarin cage, ONB-Rh cage permits semi-orthogonal lipid release (Fig. 4). Consequently, ONB-Rh cage displayed sequential photorelease of fatty acids in the presence

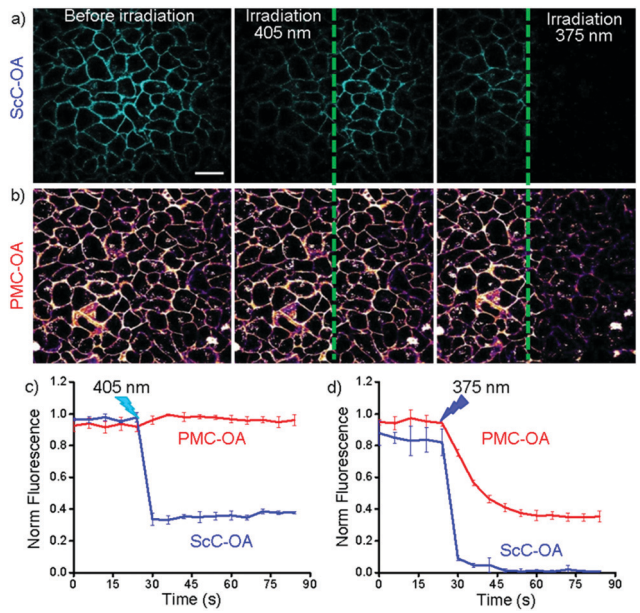

Fig. 4 Semi-orthogonal uncaging of PMC-OA in the presence of ScC-OA and sequential release of fatty acids. Fluorescence of ScC-OA (a, λ_{ex} = 405 nm) and PMC-OA (b, λ_{ex} = 559 nm) before and after exposure to 405 and 375 nm lasers for uncaging; (c) and (d) change in fluorescence of PMC-OA and ScC-OA upon subsequent irradiation with 405 and 375 nm lasers in right and left half of the image, respectively (average of three regions of interest ± SD). Scale bar is 20 μm.

of coumarin cage. Efforts are under way to further elaborate this advantage of ONB-Rh cage to study the signalling of two different lipids in the single cell.

In summary, we have presented herein the first modular design of fluorescent cages bearing split units for imaging and uncaging. We applied our cages to the simplest signalling lipid such as fatty acid. By controlling the charge on caging groups we developed caged-oleates capable of localizing at the PM or IMs. We demonstrated the photorelease of OA at the PM by monitoring GPR40 activation resulting in Ca^{2+} signalling as the read out of uncaging. The splitting of imaging and uncaging functionalities allowed us to visualize the localization of caged lipids without unintended photorelease of lipid unlike presently used coumarin caged lipids. Moreover, microscopy studies revealed the spectral compatibility of photocages with CFP- and GFP-based sensors. Additionally, the semi-orthogonal application of ONB-Rh cages to coumarin allowed the sequential photorelease of lipids. Taken together, the proof-of-principle studies anticipate that our new photocages will emerge as the tools of choice to study lipid signalling in different cellular compartments, and to study signalling of two different lipids for a given physiological effect in the same cell.

Pankaj Gaur and Oleksandr A. Kucherak were funded by IOCB postdoctoral program. The work was supported by the Czech Science Foundation (GAČR), Grant 19-21318S. We acknowledge Dr Petro Khoroshyy and Dr Dzijak Rastislav at IOCB for their support with microscopy experiments. We thank Dr Carlos Melo for critical reading of the manuscript.

Conflicts of interest

The authors declare no conflicts of interests.

Notes and references

1 K. M. Eyster, *Adv. Physiol. Educ.*, 2007, **31**, 5–16.
2 P. V. Escribá, J. M. González-Ros, F. M. Goñi, P. K. J. Kinnunen, L. Vigh, L. Sánchez-Magraner, A. M. Fernández, X. Busquets, I. Horváth and G. Barceló-Coblijn, *J. Cell. Mol. Med.*, 2008, **12**, 829–875.
3 C. Schultz, A. B. Neef, T. W. Gadella and J. Goedhart, *Cold Spring Harbor Protocols*, 2010, DOI: 10.1101/pdb.prot5458.
4 S. Lev, *Nat. Rev. Mol. Cell Biol.*, 2010, **11**, 739–750.
5 G. van Meer, D. R. Voelker and G. W. Feigenson, *Nat. Rev. Mol. Cell Biol.*, 2008, **9**, 112–124.
6 E. Muro, G. E. Atilla-Gokcumen and U. S. Eggert, *Mol. Biol. Cell*, 2014, **25**, 1819–1823.
7 A. Rutkowska and C. Schultz, *Angew. Chem., Int. Ed.*, 2012, **51**, 8166–8176.
8 S. Feng, V. Laketa, F. Stein, A. Rutkowska, A. MacNamara, S. Depner, U. Klingmuller, J. Saez-Rodriguez and C. Schultz, *Angew. Chem., Int. Ed.*, 2014, **53**, 6720–6723.
9 A. Levskaya, O. D. Weiner, W. A. Lim and C. A. Voigt, *Nature*, 2009, **461**, 997–1001.
10 E. Pastrana, *Nat. Methods*, 2010, **8**, 24.
11 J. A. Frank, M. Moroni, R. Moshourab, M. Sumser, G. R. Lewin and D. Trauner, *Nat. Commun.*, 2015, **6**, 7118.
12 J. A. Frank, D. A. Yushchenko, D. J. Hodson, N. Lipstein, J. Nagpal, G. A. Rutter, J. S. Rhee, A. Gottschalk, N. Brose, C. Schultz and D. Trauner, *Nat. Chem. Biol.*, 2016, **12**, 755–762.
13 J. A. Frank, H. G. Franquelim, P. Schwille and D. Trauner, *J. Am. Chem. Soc.*, 2016, **138**, 12981–12986.
14 J. A. Frank, D. A. Yushchenko, N. H. F. Fine, M. Duca, M. Citir, J. Broichhagen, D. J. Hodson, C. Schultz and D. Trauner, *Chem. Sci.*, 2017, **8**, 7604–7610.
15 D. Subramanian, V. Laketa, R. Müller, C. Tischer, S. Zarbakhsh, R. Pepperkok and C. Schultz, *Nat. Chem. Biol.*, 2010, **6**, 324–326.
16 P. Klan, T. Solomek, C. G. Bochet, A. Blanc, R. Givens, M. Rubina, V. Popik, A. Kostikov and J. Wirz, *Chem. Rev.*, 2013, **113**, 119–191.
17 D. Kand, L. Pizarro, I. Angel, A. Avni, D. Friedmann-Morvinski and R. Weinstain, *Angew. Chem., Int. Ed.*, 2019, **58**, 4659–4663.
18 C. Brieke, F. Rohrbach, A. Gottschalk, G. Mayer and A. Heckel, *Angew. Chem., Int. Ed.*, 2012, **51**, 8446–8476.
19 G. C. R. Ellis-Davies, *Nat. Methods*, 2007, **4**, 619.
20 L. Fournier, C. Gauron, L. Xu, I. Aujard, T. Le Saux, N. Gagey-Eilstein, S. Maurin, S. Dubruille, J.-B. Baudin, D. Bensimon, M. Volovitch, S. Vriz and L. Jullien, *ACS Chem. Biol.*, 2013, **8**, 1528–1536.
21 H. Yu, J. Li, D. Wu, Z. Qiu and Y. Zhang, *Chem. Soc. Rev.*, 2010, **39**, 464–473.
22 B. N. Goguen, A. Aemissegger and B. Imperiali, *J. Am. Chem. Soc.*, 2011, **133**, 11038–11041.
23 C. Menge and A. Heckel, *Org. Lett.*, 2011, **13**, 4620–4623.
24 J. M. Amatrudo, J. P. Olson, G. Lur, C. Q. Chiu, M. J. Higley and G. C. R. Ellis-Davies, *ACS Chem. Neurosci.*, 2014, **5**, 64–70.
25 J. A. Peterson, C. Wijesooriya, E. J. Gehrmann, K. M. Mahoney, P. P. Goswami, T. R. Albright, A. Syed, A. S. Dutton, E. A. Smith and A. H. Winter, *J. Am. Chem. Soc.*, 2018, **140**, 7343–7346.
26 I. Elamri, M. Heumüller, L.-M. Herzig, E. Stirnal, J. Wachtveitl, E. M. Schuman and H. Schwalbe, *ChemBioChem*, 2018, **19**, 2458–2464.
27 P. P. Goswami, A. Syed, C. L. Beck, T. R. Albright, K. M. Mahoney, R. Unash, E. A. Smith and A. H. Winter, *J. Am. Chem. Soc.*, 2015, **137**, 3783–3786.
28 T. Slanina, P. Shrestha, E. Palao, D. Kand, J. A. Peterson, A. S. Dutton, N. Rubinstein, R. Weinstain, A. H. Winter and P. Klán, *J. Am. Chem. Soc.*, 2017, **139**, 15168–15175.
29 M. A. Azagarsamy and K. S. Anseth, *Angew. Chem., Int. Ed.*, 2013, **52**, 13803–13807.
30 Q. Shao and B. Xing, *Chem. Soc. Rev.*, 2010, **39**, 2835–2846.
31 L. M. Heckman, J. B. Grimm, E. R. Schreiter, C. Kim, M. A. Verdecia, B. C. Shields and L. D. Lavis, *Angew. Chem., Int. Ed.*, 2016, **55**, 8363–8366.
32 A. Li, C. Turro and J. J. Kodanko, *Chem. Commun.*, 2018, **54**, 1280–1290.
33 A. Döbber, A. F. Phoa, R. H. Abbassi, B. W. Stringer, B. W. Day, T. G. Johns, M. Abadleh, C. Peifer and L. Munoz, *ACS Med. Chem. Lett.*, 2017, **8**, 395–400.
34 D. Hoglinger, P. Haberkant, A. Aguilera-Romero, H. Riezman, F. D. Porter, F. M. Platt, A. Galione and C. Schultz, *eLife*, 2015, **4**, e10616.
35 M. Mentel, V. Laketa, D. Subramanian, H. Gillandt and C. Schultz, *Angew. Chem., Int. Ed.*, 2011, **50**, 3811–3814.
36 A. Nadler, G. Reither, S. Feng, F. Stein, S. Reither, R. Muller and C. Schultz, *Angew. Chem., Int. Ed.*, 2013, **52**, 6330–6334.
37 D. Hoglinger, A. Nadler and C. Schultz, *Biochim. Biophys. Acta*, 2014, **1841**, 1085–1096.
38 D. Hoglinger, A. Nadler, P. Haberkant, J. Kirkpatrick, M. Schifferer, F. Stein, S. Hauke, F. D. Porter and C. Schultz, *Proc. Natl. Acad. Sci. U. S. A.*, 2017, **114**, 1566–1571.
39 A. Nadler, D. A. Yushchenko, R. Müller, F. Stein, S. Feng, C. Mulle, M. Carta and C. Schultz, *Nat. Commun.*, 2015, **6**, 10056.
40 S. Feng, T. Harayama, S. Montessuit, F. P. A. David, N. Winssinger, J.-C. Martinou and H. Riezman, *eLife*, 2018, **7**, e34555.
41 N. Wagner, M. Stephan, D. Höglinger and A. Nadler, *Angew. Chem., Int. Ed.*, 2018, **57**, 13339–13343.
42 S. Feng, T. Harayama, D. Chang, J. T. Hannich, N. Winssinger and H. Riezman, *Chem. Sci.*, 2019, **10**, 2253–2258.
43 G. Milligan, B. Shimpukade, T. Ulven and B. D. Hudson, *Chem. Rev.*, 2017, **117**, 67–110.
44 S. Hauke, K. Keutler, P. Phapale, D. A. Yushchenko and C. Schultz, *Diabetes*, 2018, **67**, 1986–1998.
45 J. R. Friedman, L. L. Lackner, M. West, J. R. DiBenedetto, J. Nunnari and G. K. Voeltz, *Science*, 2011, **334**, 358–362.
46 V. V. Belousov, A. F. Fradkov, K. A. Lukyanov, D. B. Staroverov, K. S. Shakhbazov, A. V. Terskikh and S. Lukyanov, *Nat. Methods*, 2006, **3**, 281–286.
47 C. F. Burant, *Diabetes Care*, 2013, **36**, S175.
48 T.-W. Chen, T. J. Wardill, Y. Sun, S. R. Pulver, S. L. Renninger, A. Baohan, E. R. Schreiter, R. A. Kerr, M. B. Orger, V. Jayaraman, L. L. Looger, K. Svoboda and D. S. Kim, *Nature*, 2013, **499**, 295.